An efficient fingerprint verification system using integrated wavelet and Fourier–Mellin invariant transform

Andrew Teoh Beng Jin[*], David Ngo Chek Ling, Ong Thian Song

Faculty of Information Science and Technology (FIST), Multimedia University, Jalan Ayer Keroh Lama, Bukit Beruang, 75450 Melaka, Malaysia

Abstract

Today, minutiae-based and image-based are the two major approaches for the purpose of fingerprint authentication. Image based approach offers much higher computation efficiency with minimum pre-processing and proves also effective even when the image quality is too low to allow a reliable minutia extraction. However, this approach is vulnerable to shape distortions as well as variation in position, scale and orientation angle. In this paper, a novel method of image based fingerprint matching based on the features extracted from the integrated Wavelet and the Fourier–Mellin Transform (WFMT) framework is proposed to remedy these problems. Wavelet transform, with its energy compacted feature is used to preserve the local edges and reduce noise in the low frequency domain after image decomposition, and hence making the fingerprint images less sensitive to shape distortion. The Fourier–Mellin transform (FMT) served to produce a translation, rotation and scale invariant feature. Multiple WFMT features can be used to form a reference invariant feature through the linearity property of FMT and hence reduce the variability of the input fingerprint images. Based on this integrated framework, a fingerprint verification system is designed. The experiments show the verification accuracy is 5.66 and 1.01% of equal error rate is achieved when multiple WFMT features are used.
© 2003 Elsevier B.V. All rights reserved.

Keywords: Fingerprint verification; Wavelet transform; Fourier–Mellin transform; Invariant features

1. Introduction

Fingerprint is the pattern of ridge and furrows on the surface of a fingertip. The pattern is formed by a set of ridgelines, which sometimes terminates (ridge-ending) or intersects (bifurcation). These ridge-ending and bifurcation form a set of features called minutiae. Various approaches of automatic fingerprint matching have been proposed in the literature. Fingerprint matching techniques can be broadly classified as being either minutiae-based or image based [1–3,6,7]. Minutiae based approach first extracts the minutiae from the fingerprint images. Then the decision is made based on the correspondence of the two sets of minutiae locations. Minutiae based approaches are the most popular ones being in almost contemporary fingerprint matching systems. This approach depends heavily on both pre-processing and post-processing operations (i.e image enhancement, directional filtering, ridge segmentation, ridge thinning, minutiae extraction, purification and point registration) in order to get reliable minutiae features [2–5]. The main drawback of the minutiae-based approach is that errors can propagate from minutiae extraction down to the decision stage [6].

Unlike minutiae extraction, image based approaches usually extract the feature directly from the raw image since a gray-level fingerprint image contains much richer, more discriminatory information compared to the minutiae locations. The minimum pre-processing requirement with this approach may also reduce the computation load. Additionally, image-based approaches may be the only viable choice, for instance, when image quality is too low to allow reliable minutia extraction [7]. However, the image based approach suffer from the two types of distortions: (1) noise, which is caused by the capturing device or by e.g. dirty fingers and (2) non-linear distortions, often produced by an incorrect finger placement over the sensing element. This causes various sub regions in the sensed image to be distorted differently due to the non-uniform pressure applied

* Corresponding author. Tel.: +606-252-3090; fax: 606-231-5604.
  E-mail address: andrew_tbj@yahoo.com, bjteoh@mmu.edu.my (A.T.B. Jin).

by the subject. Also, the variation in position, scale and orientation angle is difficult to track when using this approach [7].

In this paper, a new image-based method is proposed. By using an integrated Wavelet and Fourier–Mellin transformed feature (WFMT) the distortion and alignment problems are alleviated while retaining the advantages of the image based approach. The only pre-processing step is the reference point detection in the fingerprint image. In this proposed technique, Wavelet transform preserves the local edges and noise reduction in the low frequency domain (high energy compacted) after the image decomposition, and hence makes the fingerprint images less sensitive to shape distortion. In addition to that, the reduced dimension of the images also helps to improve the computation efficiency. Fourier–Mellin transform (FMT) produces a translation, rotation in plane and scale invariant feature. The linearity property of FMT enables multiple WFMT features to be used to form a reference invariant feature and hence reduce the variability of the input fingerprint images. Based on this integrated framework, a fingerprint verification system can be designed.

The outline of the paper is as follows: Sections 2 and 3 provide a short review of Wavelet Transform and FMT, respectively. Section 4 presents the integrated framework of Wavelet Transform and the FMT for representing the fingerprint image, while the architecture of the fingerprint verification system based on the WFMT feature is illustrated in Section 5. Section 6 presents the experimental results, discussion and the comparison with a few existing image based techniques.

2. Wavelet transform

2.1. Short review of discrete wavelet transform

The wavelet decomposition of a signal $f(x)$ can be obtained by a convolution of signal with a family of real orthonormal basis, $\psi_{a,b}(x)$

$$(W_{\psi}f(x))(a, b)$$

$$= |a|^{-\frac{1}{2}} \int_{\Re} f(x) \psi\left(\frac{x - b}{a}\right) \mathrm{d}x \, f(x) \in L^2(\Re) \qquad (1)$$

where $a, b \in \Re$ and $a \neq 0$ are the dilation parameter and the translation parameter, respectively. The basis function $\psi_{a,b}(x)$ is obtained through translation and dilation of a kernel function $\psi(x)$ known as mother wavelet [8] as defined below:

$$\psi_{a,b}(x) = 2^{-a/2}\psi(2^{-a}x - b) \qquad (2)$$

The mother wavelet $\psi(x)$ can be constructed from a scaling function, $\phi(x)$. The scaling function $\phi(x)$ satisfies the following two-scale difference equation

$$\phi(x) = \sqrt{2} \sum_n h(n)\phi(2x - n) \qquad (3)$$

where $h(n)$ is the impulse response of a discrete filter which has to meet several conditions for the set of basis wavelet functions to be orthonormal and unique [8]. The scaling function $\phi(x)$ is related to the mother wavelet $\psi(x)$ via

$$\psi(x) = \sqrt{2} \sum_n g(n)\phi(2x - n) \qquad (4)$$

The coefficients of the filter $g(n)$ are conveniently extracted from filter $h(n)$ from the following relation

$$g(n) = (-1)^n h(1 - n) \qquad (5)$$

The discrete filters $h(n)$ and $g(n)$ are the quadrature mirror filters (QMF), and can be used to implement a wavelet transform instead of explicitly using a wavelet function.

For 2D signal such as image, there exists an algorithm similar to the one-dimensional case for two dimensional wavelets and scaling functions obtained from one-dimensional ones by tensorial product. This kind of two-dimensional wavelet transform leads to a decomposition of approximation coefficients at level $j - 1$ in four components: the approximations at level j, and the details in three orientations (horizontal, vertical and diagonal)

$$L_j(m, n) = [H_x * [H_y * L_{j-1}]_{\downarrow 2,1}]_{\downarrow 1,2}(m, n) \qquad (6)$$

$$D_{j \text{ vertical}}(m, n) = [H_x * [G_y * L_{j-1}]_{\downarrow 2,1}]_{\downarrow 1,2}(m, n) \qquad (7)$$

$$D_{j \text{ horizontal}}(m, n) = [G_x * [H_y * L_{j-1}]_{\downarrow 2,1}]_{\downarrow 1,2}(m, n) \qquad (8)$$

$$D_{j \text{ diagonal}}(m, n) = [G_x * [G_y * L_{j-1}]_{\downarrow 2,1}]_{\downarrow 1,2}(m, n) \qquad (9)$$

where $*$ denotes the convolution operator, $\downarrow 2, 1$ ($\uparrow 2, 1$) subsampling along the rows (columns), H and G are a low pass and bandpass filter, respectively. This decomposition algorithm can also be illustrated by the block diagram in Fig. 1.

2.2. Fingerprint images in wavelet domain

As described in Section 2.1, a multiresolution representation can provide a hierarchical framework for interpreting the image information and the wavelet transform can be used to decompose the image into a multiresolution
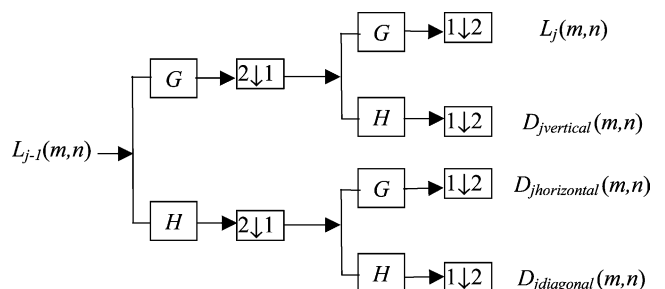

Fig. 1. Decomposition of $L_{j-1}(m, n)$ into four quarter-size images by using the conjugate filter H and G.

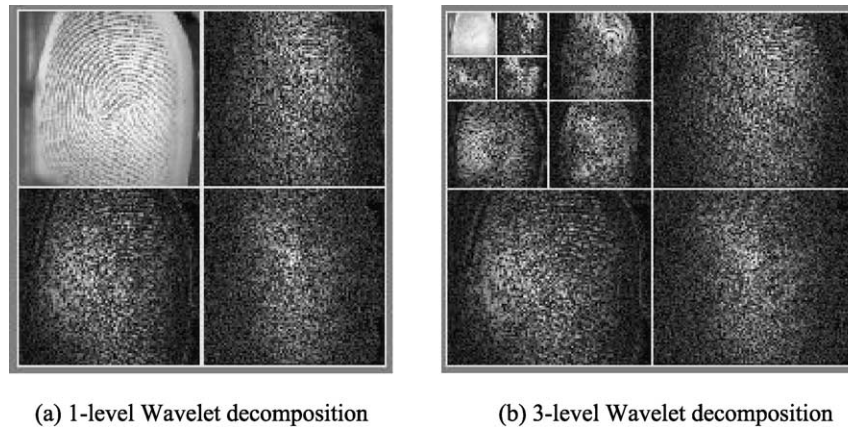(a) 1-level Wavelet decomposition   (b) 3-level Wavelet decomposition

Fig. 2. 2D wavelet decomposition of a fingerprint image.

representation. Fig. 2(a) shows the decomposition process by applying the 2D wavelet transform on a fingerprint image in level 1. Similarly, two levels of the wavelet decomposition as shown in Fig. 2(b) by applying wavelet transform on the low-frequency band sequentially.

In Fig. 2(a), the subband L_1 corresponds to the low-frequency components in both vertical and horizontal directions of the original images, making it the low-frequency subband of the original image. The subband $D_{1horizontal}$ corresponds to the high-frequency component in the horizontal direction (horizontal edges). A similar interpretation is made on the subbands $D_{1\ vertical}$ (vertical edges) and $D_{1\ Diagonal}$ (both directions).

For fingerprint images, the ridge structure can be viewed as an oriented texture pattern, which often runs parallel in omni direction. According to wavelet theory, the wavelet transform conserves the energy of signals and redistributes this energy into more compact form. It is commonly found that most of the energy content will be concentrated in low frequency subband, L_j if compare to high frequency subbands, D_j. Obviously, D_j's are not suitable to represent the ridge structure because of their low energy content and its high pass feature that tends to enhance the edges detail, including noise and the shape distortion whereas the subband L_j is the smoothed version of original image and

thus helps to reduce the influence of noise on one hand, and on the other hand it also preserves the local edges well which helps to capture the features that insensitive to the small distortion.

However, how well is the L_j can preserve the energy is depend to the chosen wavelet bases. By using the 1st level decomposed fingerprint image that shown in Fig. 2 with various wavelet bases, the normalised energy distributions are shown in Table 1. The results show that the orthogonal/biorthogonal and high order wavelet bases are able to preserve the energy efficiently in subband L_j which is only quarter size of the original image. In turn, the computational complexity will be reduced dramatically by working on a lower resolution image. This makes the wavelet approach differ from the other common techniques that also reduce the noise as well as resolution reduction, such as spatial filters with dyadic down-sampling. Table 2 shows the energy leakage of the spatial filter followed the way of wavelet decomposition that shown in Fig. 1 where H and G are replaced with the spatial filters, i.e filtering followed with dyadic down-sampling. This implies the information content in the fingerprint images will be lost. On the other hand, verification results in Section 6.2 will be another vindication of the observation.

Table 1
Energy distribution of various wavelet bases in four subband images

Wavelet bases			Normalised energy distribution (%)			
Type	Orthogonality	Symmetry	L_j	$D_{1horizontal}$	$D_{1vertical}$	$D_{1diagonal}$
Haar	Orthogonal	No	99.348	0.251	0.377	0.024
Daubechies 4	Orthogonal	No	99.856	0.060	0.080	0.003
Daubechies 8	Orthogonal	No	99.913	0.040	0.045	0.002
Symlets 4	Orthogonal	Near	99.856	0.060	0.080	0.003
Symlets 8	Orthogonal	Near	99.907	0.042	0.049	0.002
Discrete Meyer	Biorthogonal	Yes	99.936	0.030	0.033	0.002
Spline Bior 1.1	Biorthogonal	Yes	99.348	0.251	0.3770	0.024
Spline Bior 5.5	Biorthogonal	Yes	99.903	0.044	0.0494	0.004
Discrete Morlet	No	Yes	94.363	2.218	2.327	1.092

Table 2
Energy leakage in the dyadic sub-sampled fingerprint images after the filtering

Spatial filter	Energy content (%) after the first level of dyadic sub-sampling
Mean filter	88.834
Gaussian filter	89.401
Median filter	88.189
Unsharp masking filters	90.261

3. Fourier–Mellin invariant features

In the fingerprint authentication, the varying position, scale and the orientation angle of the fingerprint image during the capturing time may severely reduce performance, as shown in Fig. 3. These alignment problems can be solved by transforming a fingerprint image into an invariant feature.

Various translation, rotation and scale invariant methods such as integral transforms, moment invariants and Neural Network approaches have been proposed [9]. These techniques provide good invariance theories but suffer from the presence of noise, computation complexity or accuracy problem [9]. In this paper, a well-known translation, scaling and rotation invariant function which called FMT is adopted. FMT performs well under noise and can be applied efficiently by using Fast Fourier Transform [10]. FMT is translation invariant and represents rotation and scaling as translations along the corresponding axes in parameter space.

Consider an image $f_2(x, y)$ that is a rotated, scaled and translated replica of $f_1(x, y)$,

$$f_2(x, y) = f_1[\sigma(x \cos \alpha + y \sin \alpha)$$
$$- x_0, \ \sigma(-x \sin \alpha + y \cos \alpha) - y_0] \tag{10}$$

where α is the rotation angle, σ the uniform scale factor, and x_0 and y_0 are translational offsets. The Fourier Transform of $f_1(x, y)$ and $f_2(x, y)$ are related by

$$F_2(u, v) = e^{-j\phi_s(u,v)}\sigma^{-2}[F_1[\sigma^{-1}(u \cos \alpha + v \sin \alpha),$$
$$\sigma^{-1}(-u \sin \alpha + v \cos \alpha))]] \tag{11}$$

where $\phi_s(u, v)$ is the spectra phase of the image $f_2(x, y)$. This phase depends on the translation, scaling and rotation, but the spectral magnitude

$$|F_2(u, v)| = \sigma^{-2}|F_1[\sigma^{-1}(u \cos \alpha + v \sin \alpha),$$
$$\sigma^{-1}(-u \sin \alpha + v \cos \alpha))]| \tag{12}$$

is translation invariant.

Equation (12) shows that a rotation of the image rotates the spectral magnitude by the same angle, and that a scaling by σ scales the spectral magnitude by σ^{-1}. Rotation and scaling can be decoupled by defining the spectral magnitudes of f_1 and f_2 in the polar coordinates (θ, r),

$$f_{2p}(\theta, r) = |F_2(r \cos \theta, r \sin \theta)|,$$
$$f_{1p}(\theta, r) = |F_1(r \cos \theta, r \sin \theta)| \tag{13}$$

By applying some appropriate trigonometry identities, one can obtain

$$f_{2p}(\theta, r) = \sigma^{-2} f_{1p}(\theta - \alpha, r/\sigma) \tag{14}$$

Hence an image rotation shifts the function $f_{1p}(\theta, r)$ along the angular axis. A scaling is reduced to a scaling of the radial coordinate and to a magnification of the intensity by a constant factor σ^2. Scaling can be further reduced to a translation by using a logarithmic scale for the radial coordinate, thus

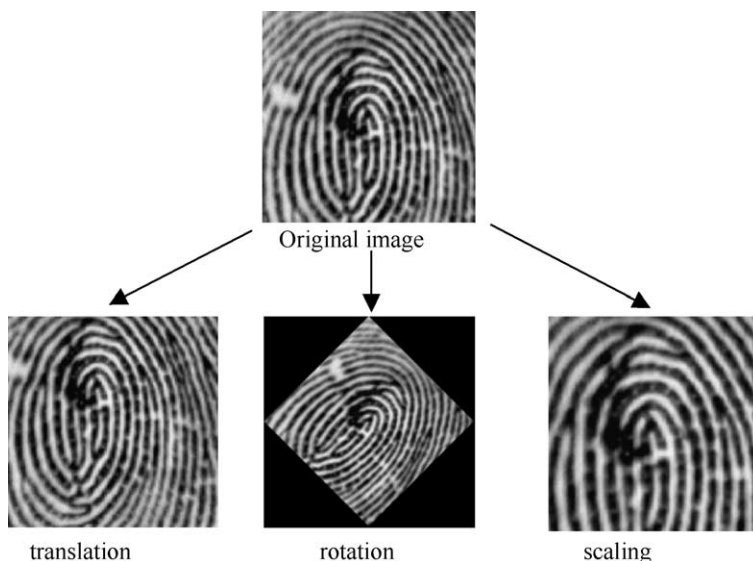$$f_{2pl}(\theta, \lambda) = f_{2p}(\theta, r) \tag{15}$$

Fig. 3. Three general errors that may occur in fingerprint authentication system.

and

$$f_{2pl}(\theta, \lambda) = f_{2p}(\theta, r) = \sigma^{-2} f_{1pl}(\theta - \alpha, r - \eta) \tag{16}$$

where, $\lambda = \log(r)$ and $\eta = \log(\sigma)$. In this polar-logarithmic representation, both rotation and scaling are reduced to translation. By Fourier transforming the polar-logarithm representations, Eqs. (15) and (16),

$$F_{2pl}(\zeta, \xi) = \sigma^{-2} e^{-j2\pi(\zeta\eta + \xi\lambda)} F_{1pl}(\zeta, \xi) \tag{17}$$

where

$$F_{1pl}(\zeta, \xi) = \int_{-\infty}^{\infty} \int_{0}^{2\pi} f_{1pl}(\theta, \lambda) e^{j(\zeta\lambda + \xi\theta)} d\theta d\lambda \tag{18}$$

thereby rotation and scaling now appear as phase shifts. This technique decouples images rotation, scaling and translation, and is therefore very efficient numerically.

4. Integrated framework of wavelet transform and Fourier–Mellin transform

The integrated framework of WFMT produces an invariant, distortion and noise insensitive feature. In addition to that, reduce the resolution of the image decrease the computation of the feature generation. In this paper, 2 levels decomposition are performed on a fingerprint image with size 128×128 due to the consideration that too coarse resolution is inappropriate, as down sampling process would eliminates the orientation characteristics of ridge structures. Experiment results in Section 6.2 show that L_1 subband (size 64×64) with Spline Bior 5.5 gives the best performance whereas the usage of L_2 seems to decrease the performance.

The fingerprint image with the low-frequency subband representation is then subjected to log-polar mapping and Fast Fourier Transforming as described in Section 3. However, the result stated for the continuous case does not carry over exactly to the discrete case. Some artifacts may be introduced due to the sampling and truncation if the implementation is not done with care [11,12]. The first implementation difficulty consists of the numerical instability of coordinates near to the origin. Here care needs to be taken in selecting the starting point of the logarithm resampling, since $\lim_{r \to 0} \ln r = -\infty$. Therefore a high-pass filter is apply on the logarithm spectra [13],

$$H(x, y) = (1.0 - \cos(\pi x) \cos(\pi y))(2.0 - \cos(\pi x) \cos(\pi y)) \tag{19}$$

with $-0.5 \leq x, y \leq 0.5$.

The dynamic range of the spectral magnitude is usually large and the values of the spectral magnitude at the two ends of the radial axis differ by several orders of magnitude. This discontinuity can cause artifacts but can suppress by applying a Hanning window to the input images.

In the proposed framework, FMT is based on Fourier Transform theory, which has a linear property as below:
If $f_i \in \Re^2$, $a \in \Re$, then

$$F_{pl}\left\{ \sum_{i=1}^{m} a_i f_i \right\} = \sum_{i=1}^{m} F_{pl}\{a_i f_i\} \tag{20}$$

This implies that multiple m WFMT features can be used to form a reference WFMT feature and just only one representation per user needs to be stored in the database. The representation for each user, WFMT$_{Ui}$ can be formulated as follow:

$$\text{WFMT}_{Ui} = \frac{1}{m} \sum_{j=1}^{m} \text{WFMT}_{j}^{i} \tag{21}$$

where WFMT$_{j}^{i}$ is the invariance feature of the jth finger image of the ith person. Producing a WFMT$_U$ feature from different training images, could relax various variability's that occur during the acquisition process, such as sharp distortion and noise.

The block diagram of the WFMT feature representation is shown in Fig. 4.

5. Fingerprint verification system based on WFMT features

A fingerprint verification system checks whether a person really is who he claims to be. A person first identifies himself by e.g. an ID or smart card. Then, the user puts his or her finger on a sensor. A typical image based fingerprint verification system comprises the following sub modules: Pre-processing, such as reference point detection, feature extraction and classification. The verification system consists of two stages, namely, training stage and verification stage. Training stage represents a set of the template images as WFMT feature, label and store them into a database. Verification stage converts an input image into WFMT feature, and then matches it with the claimant fingerprint image stored in the database to get the dissimilarity measure. Thereafter, the similarity measure is compared to a predefined threshold to determine whether a claimant should be accepted. Fig. 5 shows the system block diagram.

In the verification stage, the comparison of two fingerprints must be based on the same reference point (or core point). The method proposed in [14] is opted to detect the reference point. In this algorithm, core point of a fingerprint is defined as the point of maximum curvature in the fingerprint image; the coupling of the modified averaged square directional field (MASDF) with morphological operation enable it to detect the five Henry classes [15] of the fingerprint images, as illustrated in Fig. 6. At first, an input fingerprint will be divided into non-overlapping blocks of size 5×5. In each block, the x and y magnitudes of the gradient, G_x and G_y at each pixel in each block were
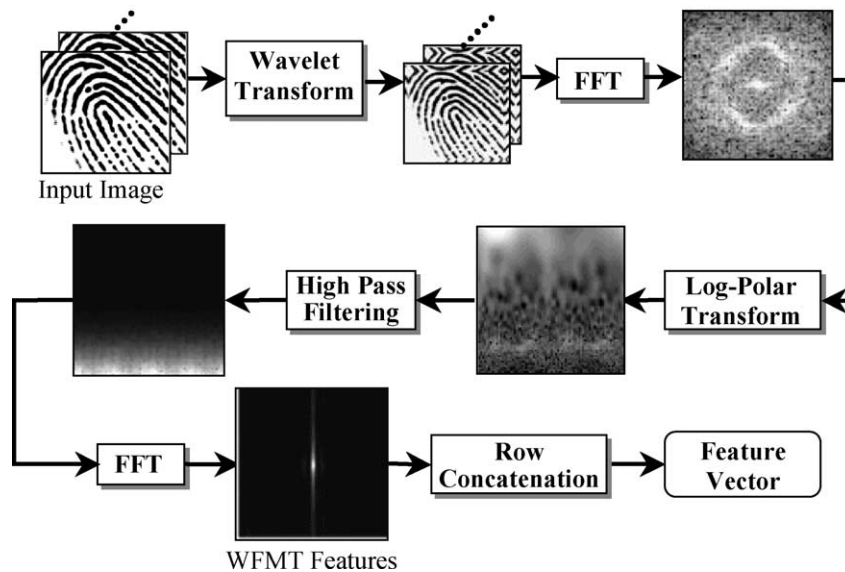
Fig. 4. Block diagram of generating the WFMT features.

determined. With each block, slope that perpendicular to the local gradient orientation of each block will be computed to produce a MASDF. In the MASDF, the blocks with slopes value ranging from 0 to $1/2\pi$ will be sought and marked as '1' otherwise '0' was assigned to produce a binary pattern. However, the binary pattern shows a lot spurious points or cluster area that may lead to the false detection core point. In order to rectify this problem, mathematical morphological operations are performed to 'repairs' the estimate by removing small areas, thus creating more compact cluster and thus easier to pinpoint the core point. [14] reported only 3.13% of false core point detection rate was obtained in 160 FVC2000 (Set B) fingerprint images.

For the dissimilarity matching, a simple Euclidean distance metric is employed instead of more complex classifiers such as neural network or Support Vector Machine (SVM). This is because we are more concern about the effectiveness of using WFMT features rather than the classification technique in the experiment. Besides that, k-Nearest Neighbourhood (k-NN) also has been adopted in order to compare with the system that reported in the literature.

The computation complexity of WFMT in verification task could be estimated as follow: Let the number of pixels found in an image is n. The complexity of the wavelet transform is then $O(n \times \log n)$. Suppose the dimension of wavelet subband, L_1 is n' where $n' < n$, the complexity of applying FMT on the L_1 is $O(n \times \log n')$. Eventually, the complexity for verifying a training images is $O(n')$. Therefore, the computational complexity for WFMT is $O(n \times \log n + 2n \times \log n')$ in the training stage and $O(n \times \log n + 2n \times \log n + n')$ in the recognition stage.

6. Experiments and discussion

The experimental results presented in this section are divided into five parts. The first part details the experiment protocol of the proposed method. The second part compares the performance of different wavelet and spatial filters to form the WFMT feature. Part three evaluates on using multiple training WFMT features to form a reference WFMT feature. The next part evaluates the translation, scale and rotation on the plane invariant characteristic of WFMT feature. Finally, a comparison between the proposed method and the existing methods is presented.
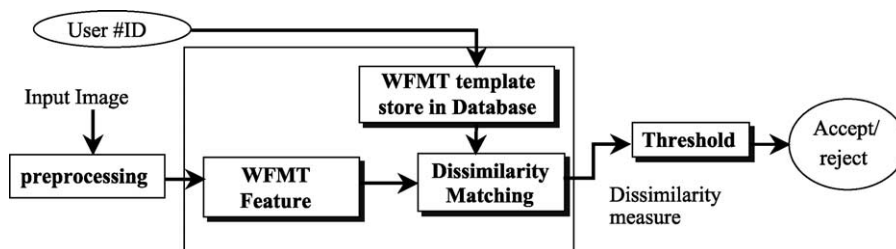

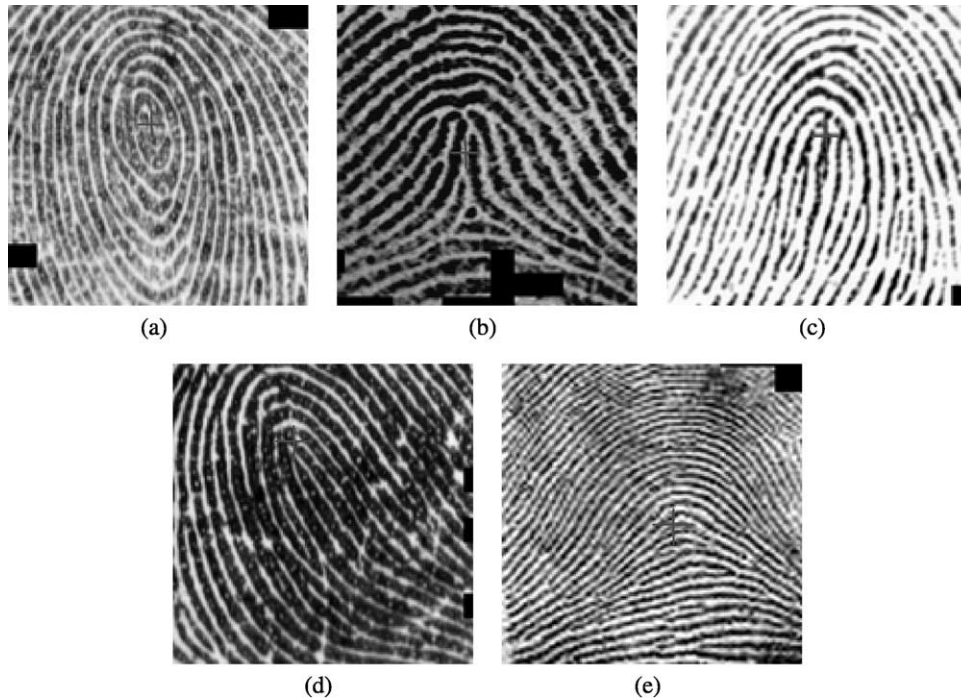Fig. 5. Block diagram of the Fingerprint Verification System.

Fig. 6. Core point extraction for example from each of the five Henry classes with. (a) Whorl. (b) Tented arch. (c) Left Loop. (d) Right Loop and (e) Arch.

6.1. Experiment setup

In fingerprint research community, there are only a few benchmarks are available, namely NIST, FVC 2000 and FVC 2002 databases. NIST databases containing thousands of scanned inked impressions of fingers. Since these images notably differ from those acquired electronically, they are not well suited for the testing contemporary (online) fingerprints system. FVC 2000 and FVC 2002 databases were established with the aim of providing a benchmark to determine the state-of-the-art in fingerprint recognition application, where the finger impressions were acquired by using modern capacitive and optical scanners [17].

In this paper, the algorithm is evaluated on images taken from FVC 2002 (Set A), which is available in DVD included in [16]. FVC2002 (Set A) provided four different fingerprint databases: DB1, DB2, DB3 and DB4, three of these databases are acquired by various sensors, low-cost and high quality, optical and capacitive. 90 volunteers were randomly partitioned into three groups (30 person each); each group was associated to a DB and therefore to a different fingerprint scanners. The fourth database contains synthetically generated images. Preparation procedure of FVC 2002 has been explained in detail in [17]. All databases in FVC2002 (Set A) contain 8 impressions of 100 different fingers, hence 800 images in total. However, the comparison only can be done if both fingerprint images contain their respective core points, as mentioned in Section 5, but 2 out of 8 impressions for each finger in FVC2002 have no core point due to the exaggerate displacement. In our experiments, these two impressions were excluded and hence, there are only 6 impressions per finger yielding 600

(6×100) fingerprint images in total for each database. Every finger image will be performed core point detection and a 128×128 square region centred in the reference point of the fingerprint images can be cropped as shown in Fig. 7. Even though some false core points were detected but they are not deviate too much from the actual core point location. It is commonly known that the slight translation is invariant under FMT and thus we still included those false detected core point images as our experimenting subjects. The experiments were conducted separately for DB1, DB2 and DB3, particularly in Section 6.2 due to their fingerprint images are acquired by using different type of sensor.

For the performance evaluation, a False Acceptance Rate (FAR) and a False Rejection Rate (FRR) test is performed. The FAR and FRR are defined as below:

$$FAR = \frac{\text{Number of accepted imposter claims}}{\text{Total number of imposter accesses}} \times 100\% \quad (22)$$

$$FRR = \frac{\text{Number of rejected genuine claims}}{\text{Total number of genuine accesses}} \times 100\% \quad (23)$$

These two measurements may yields another performance measure known as Total Success Rate (TSR):

$$TSR = \left(1 - \frac{FAR + FRR}{\text{Total number of accesses}}\right) \times 100\% \quad (24)$$

However, this performance indicator may somehow misleading due to the great imbalance number of genuine and imposter distribution, and it is better to adopt Equal Error Rate (EER) when FAR = FRR or alternatively EER = (FAR + FRR)/2.

Fig. 7. Samples of cropped fingerprint image that based on the reference point detected from DB1, DB2 and DB3, respectively.

6.2. Performance evaluations on different wavelet basis

This section shows the verification performance of various combinations of the wavelet basis in the WFMT feature. For each database, an FRR and an FAR test is performed. For the FAR test, the first impression of each finger is matched against the first impression of all other fingers and the same matching process was repeated for subsequent impressions, leading to 29,700 ($4{,}950 \times 6$) imposter attempts. For the FRR test, each impression of each finger is matched against all other impressions of the same finger, leading to 1,500 (15 attempts of each finger $\times 10$). The first experiments in this section are performed on DB1 which acquired by using optical sensor.

From the Table 3, wavelet basis with Spline biorthogonal order 5.5, level 1 attains the best performance, which is 5.93, 5.38, 94.60 and 5.66% of FAR, FRR, TSR and EER, respectively. This is inline to the observations that found in Table 1 which shown the Spline bior 5.5 wavelet compacted the highest energy in L_1. The other high order orthogonal wavelets such as Daubechies 8, Symlet 8 and discrete Meyer, which is also superior in the energy preservation in L_1, achieved the relatively good verification rate as well. In contrary, the non-orthogonal wavelet, i.e discrete Morlet and other normal spatial filters that unable to preserve the energy were poorly performed. Generally, there is a direct relation in between the ability of a wavelet to preserve the energy in dyadic sub-sampling fingerprint images and the discrimination power in WFMT as depicted in Fig. 8. However, for this application, it does not really matter if the wavelet is symmetric or not.

It also can be observed that experimental result in level 2 generally is poor compare to level 1. This indicates that the excessive down sampling process eliminates the orientation characteristics of ridge structures of the coarser image or in other words, lesser energy is maintained; hence lower the discrimination power of WFMT. On the other hand, the performance is inferior when only sole Fourier–Mellin transform is applied, i.e 15.53, 17.75, 82.36 and 16.64% of FAR, FRR, TSR and EER, respectively.

By using the chosen wavelet basis - decomposition level 1 with Spline Bior 5.5, experiments were performed on DB2 and DB3, and the results are tabulated in the Table 4.

Experiment results show that DB3 is slightly inferior compare to the DB1 and DB2. This implies that the usage of sensor with different technology might affect the performance of an image based fingerprint recognition algorithm.

6.3. Forming a reference WFMT feature by using multiple training WFMT features

The linearity property of FMT ensures that multiple WFMT features can be used to form a reference WFMT feature, which is able to relax the variability that occurred during the acquisition process. In this section,

Table 3
Comparative result of verification rate

| Filter	Decomposition level	FRR (%)	FAR (%)	TSR (%)	EER (%)
None (sole FMT)	–	15.533	17.751	82.356	16.642
Mean filter	–	20.000	21.737	78.346	20.869
Gaussian filter	–	19.600	19.077	80.897	19.339
Median filter	–	19.733	18.815	81.141	19.274
Unsharp masking filters	–	15.867	16.862	83.186	16.364
Haar	1	7.333	7.923	92.106	7.628
	2	13.000	13.737	86.298	13.369
Daubechies 4	1	7.067	7.195	92.811	7.131
	2	12.067	12.939	87.103	12.503
Daubechies 8	1	7.067	6.700	93.282	6.884
	2	12.000	12.943	87.103	12.471
Symlet 4	1	6.667	6.707	93.295	6.687
	2	12.067	12.939	87.103	12.503
Symlet 8	1	6.600	6.488	93.506	6.544
	2	12.067	12.939	87.103	12.503
Discrete Meyer	1	6.733	6.700	93.298	6.717
	2	11.667	11.165	88.811	11.416
Spline Bior 1.1	1	6.667	6.707	93.295	6.687
	2	11.400	12.051	87.981	11.725
Spline Bior 5.5	1	5.933	5.380	94.593	5.657
	2	11.000	10.279	89.686	10.640
Discrete Morlet	1	11.400	11.990	88.038	11.695
	2	16.200	17.306	82.747	16.753
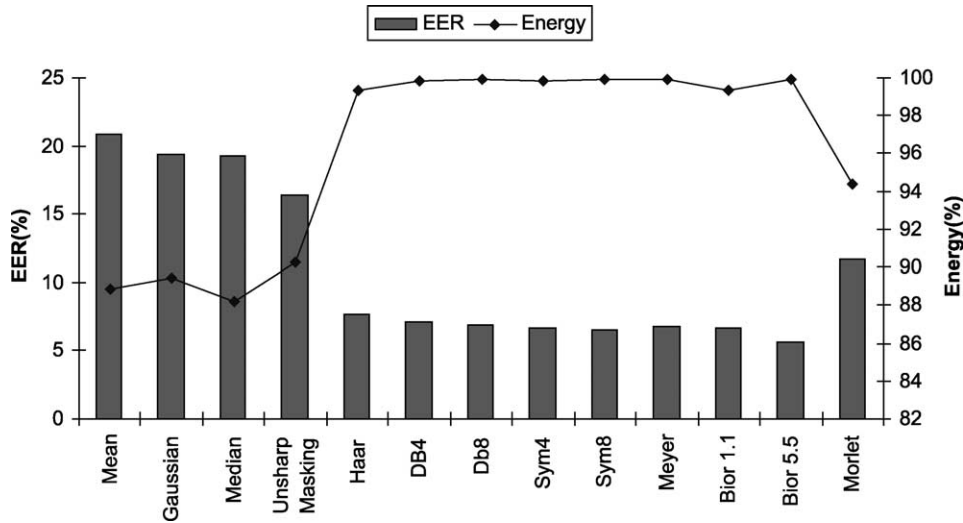
Fig. 8. Relation in between the verification rate (EER) and the energy preservation in dyadic sub-sampling fingerprint images.

the experiments were conducted by using 1–4 and 5 training images per person from DB1 to form a WFMT feature template while 6th impression is treated as the testing image to maintain the consistency of the comparison. For the FAR test, a WFMT feature template that formed by m training image(s), where $m = 1, ..., 5$ is matched against the 6th impression of all other fingers produced 9900 (100×99) imposter attempts. For the FRR test, each impression of WFMT feature template is matched against all 6th impressions of the same finger, leading 100 genuine attempts. Tables 5 and 6 show the configurations for this experiment and their results, respectively.

Table 6 shows that the verification rate in terms of EER decreases consistently when multiple training WFMT features are used. The best verification rate is obtained when four training WFMT features are used. The comparison in terms of Receiving Operating Curve (ROC) also depicted in Fig. 9. Also note that even though more than one image are used to form the reference WFMT feature, it would not increase the system and recognition complexity because only one reference WFMT is stored in database.

6.4. Invariant characteristic of WFMT feature

This section demonstrates the invariant characteristic of the WFMT feature. A test database is arranged according to the experiment setting on DB1 in Section 6.2 but the optimum wavelet setting, which is in decomposition level 1

and Spline Bior 5.5 is used. However, each testing image is rotated on plane from -90 to $90°$ with the increasing step $20°$ while training images are remain unchanged, i.e $0°$. Results in Table 7 shows the high verification rate for rotated testing images in between -30 and $30°$ and the performance drop significantly when the rotation angle exceed $\pm 30°$. These results demonstrated that the WFMT feature is invariant to rotation on the plane in within certain degree.

The translation problem may occur due to the automatic reference point detection algorithm (as mentioned in Section 5) may not always detect the reference point correctly but deviate from the actual location of the reference point. The scaling problem may also arise from

Table 5
Configurations for the experiments

Setting	Training images	Number of genuine attempts	Number of imposter attempts
1	1st	100	$100 \times 99 = 9900$
2	1st + 2nd	100	$100 \times 99 = 9900$
3	1st + 2nd + 3rd	100	$100 \times 99 = 9900$
4	1st + ⋯ + 4th	100	$100 \times 99 = 9900$
5	1st + ⋯ + 5th	100	$100 \times 99 = 9900$

Table 6
Verification accuracy when reference WFMT feature is formed by multiple training WFMT feature

Setting	FAR (%)	FRR (%)	TSR (%)	EER (%)
1	6.000	5.869	94.130	5.934
2	4.000	3.949	96.050	3.975
3	3.000	3.253	96.750	3.126
4	1.000	1.020	98.980	1.010
5	2.000	2.242	97.760	2.121

Table 4
Verification results for DB2 and DB3

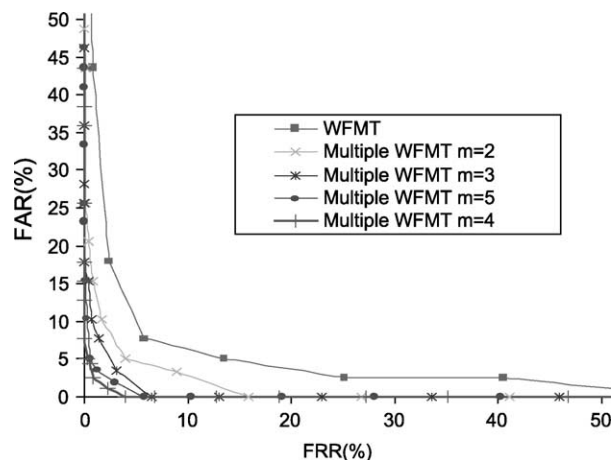| Database in FVC2002 (SetA)	FRR (%)	FAR (%)	TSR (%)	EER (%)
DB1 (Optical sensor)	5.933	5.380	94.593	5.657
DB2 (Optical sensor)	5.400	5.219	94.772	5.309
DB3 (Capacitive sensor)	8.800	7.875	92.080	8.338

Fig. 9. ROC for the comparison in between WFMT and multiple WFMT.

the uneven placement of the fingerprint in the sensor. In this paper, translation and scaling problems are addressed indirectly from the experiments result that reported in Sections 6.2, 6.3 and 6.4.

6.5. Comparison with other techniques in literature

This section presents the comparison in between the proposed method with the image based approaches found in the literature, based on the Tico et al. [7] and Lee's [18] work. Tico et al. [7] described each fingerprint with a subset of band filtered images containing wavelet coefficients. With the wavelet decomposition, a set of wavelet coefficients that characterize the fingerprint texture and the orientation can be obtained. Consequently, a set of compact feature vectors are formed using the simple statistical measures while Lee [18] proposed to use Gabor filter based features, which directly extracted from grey scale level fingerprint images as the input vector. These two papers used k nearest neighbour (k-NN) classifier to test their technique by using Biometrics System Lab database [19]. Biometrics System Lab database, contains 21 person fingerprint images and each person consists of 8 impressions. However, there are 20 person images are chosen in the experiments because there is no core point can

Table 7
Performance comparison for rotation invariant of WFMT feature

Rotated angle (testing image)	FRR (%)	FAR (%)	TSR (%)	EER (%)
$-90°$	24.710	24.953	75.019	24.831
$-70°$	13.806	14.636	85.381	14.221
$-50°$	12.968	13.391	86.609	13.179
$-30°$	10.129	9.084	90.849	9.607
$-10°$	7.548	7.916	92.090	7.732
$0°$	5.933	5.380	94.593	5.657
$10°$	8.194	8.125	91.859	8.159
$30°$	9.161	8.343	91.603	8.752
$50°$	13.355	11.350	88.532	12.353
$70°$	17.742	18.926	81.103	18.334
$90°$	25.355	26.300	73.705	25.827

Table 8
Comparative results of k-NN recognition rate

Method	1-NN (%)	2-NN (%)	3-NN (%)
Proposed method (setting 1)	94.3	97.9	100
Proposed method (setting 4)	100	100	100
Tico et al. [7] with Symmlet order 8	100	100	100
Lee and Wang [18] with Gabor magnitude and 8 orientations	90.9	94.4	96.5

be found for one person. Hence, there are 160 (20×8) images could be obtained. In order to conform the experiment setting that described in the papers mentioned above, the experiments done in Section 6.3 is reevaluated in recognition mode, using k-NN as the classifiers instead of Euclidean distance metrics as Biometrics System Lab database is adopted. However, only setting 1, which only one image is used to form the WFMT features and setting 4, where four images are used which yield the best performance are chosen. Table 8 below shows the comparative results in between the methods discussed above. Note that only the best results achieved that reported in [7] and [18] are taken to compare with the proposed method.

From Table 8, the proposed method in setting 1 exhibits the better recognition rate compare to Lee and Wang's method, while shows slightly inferiors compare to Tico et al. approach. Setting 4 achieved the comparable outcome with the Tico et al. approach. However, both papers did not mention about the possibility of their method able to be invariant to translation, scale and rotation.

7. Conclusions

An integrated framework that combined WFMT in the fingerprint verification system is presented in this paper. The proposed approach is simple in the pre-processing process, where only reference point detection involved. The complexity and computational of this integrated wavelet and Fourier–Mellin framework also are significantly low compare to the minutiae-base approach because of the available of Fast Wavelet Transform and Fast Fourier Transform. The EER of the proposed method is under 5.66% and also proves its rotation invariant property if the rotation angle not exceed $\pm 30°$, and indirectly to translation invariant if detected core point of the fingerprint is not deviate too much from the actual location. The extensibility of this method also able to achieve low EER to 1.01% if more than one training images are included.

References

[1] D. Roberge, C. Soutar, B.V.K.V. Kumar, Optimal correlation filter for fingerprint verification, SPIE vol. 3386 (1998).

[2] A.K. Jain, L. Hong, S. Pankanti, R. Bolle, An identity authentication system using fingerprints, Proc. IEEE 85 (9) (1997) 1365–1388.

[3] [.3.].S. Prabhakar, J. Wang, A.K. Jain, S. Pankanti, R. Bolle, Minutiae verification and classification for fingerprint matching, Proc. 15th Int. Conf. Pattern Recogn., Barcelona, September 3–8 1 (2000) 25–29.

[4] F. Zhao, X. Tang, Preprocessing for skeleton-based fingerprint minutiae extraction, Int. Conf. Imaging Science, Systems, and Tech. (CISST'02), Las Vegas, Nevada, USA, June 24–27 (2002).

[5] F. Zhao, X. Tang, Duality-based Post-processing for fingerprint minutiae extraction, Proc. Int. Conf. Inf. Security, Shanghai, China July (2002).

[6] A.M. Bazen, G.T.B. Verwaaijen, S.H. Gerez, L.P.J. Veelenturf, B.J.V.D. Zwaag, Correlation-based fingerprint verification system, Proc. ProRISC, Veldhoven, The Netherlands, November (2000).

[7] M. Tico, E. Immonen, P. Ramo, P. Kuosmanen, J. Saarinen, Fingerprint recognition using wavelet features, Proc. IEEE Int. Symp. Circuits Sys. 2 (2001) 21–24.

[8] S. Mallat, A Wavelet Tour of Signal Processing, Acadermic Press, San Diego, 1998.

[9] J. Wood, Invariant pattern recognition: a review, Pattern Recogn. 29 (1) (1996) 1–17.

[10] A. Grace, M. Spann, A comparison between Fourier–Mellin Descriptors and moment based features for invariant object recognition using neural networks, Pattern Recogn Lett. 12 (1991) 635–643.

[11] R.J. Schalkoff, Digital Image Processing and Computer Vision, Wiley, New York, 1989, pp. 279–286.

[12] R.N. Bracewell, The Fourier Transform and Its Application, McGraw-Hill, New York, 1986.

[13] B.S. Reddy, B.N. Chatterji, An FFT-based Technique for Translation, Rotation and Scale-Invariant Image Registration, IEEE Trans. Image Process. 5 (8) (1996) 1266–1271.

[14] Andrew Teoh, T.S. Ong, N.C.L. David, and Y.W. Sek. 2003. Automatic Fingerprint Center Point Determination, 16th Australian Joint Conference on Artificial Intelligence (AI'03), 2–5, December, Perth Australia. Lecture Notes on Artificial Intelligent, Springer-Verlag, 2903, p. 633–640. T.D. Gedeon, Lance Chun Che Fung (Eds.).

[15] E.R. Henry, Classification and Uses of Fingerprints, George Routledge and Sons, London, 1990.

[16] D. Maltoni, D. Maio, A.K. Jain, S. Prabhakar, Handbook of Fingerprint Recognition, Springer, New York, 2003.

[17] D. Maio, D. Maltoni, R. Cappelli, J.L. Wayman, A.K. Jain, FVC2002: second fingerprint verification competition, Proc. Int. Conf. Pattern Recogn., Quebec City, August 11–15 (2002) 2002.

[18] C.J. Lee, S.D. Wang, Fingerprint feature extraction using Gabor Filters, Electron. Lett. 35 (4) (1999) 288–290.

[19] Biometric Systems Lab. University of Bologna. Cesena-Italy. http://www.csr.unibo.it/research/biolab/.